

Cell surface fluctuations studied with defocusing microscopyU. Agero,¹ C. H. Monken,¹ C. Ropert,² R. T. Gazzinelli,^{2,3} and O. N. Mesquita¹¹*Departamento de Física, ICEX, Universidade Federal de Minas Gerais, Caixa Postal 702, Belo Horizonte, CEP 30123-970 Minas Gerais, Brazil*²*Centro de Pesquisas René Rachou, Fiocruz Belo Horizonte, Minas Gerais, Brazil*³*Departamento de Bioquímica e Imunologia, ICB, Universidade Federal de Minas Gerais, Belo Horizonte, CEP 30123-970 Minas Gerais, Brazil*

(Received 27 December 2002; published 7 May 2003)

Phase objects can become visible by slightly defocusing an optical microscope, a technique seldom used as a useful tool. We revisited the theory of defocusing and apply it to our optical microscope with optics corrected at infinity. In our approximation, we obtain that the image contrast is proportional to the two-dimensional (2D) Laplacian of the phase difference introduced by the phase object. If the index of refraction of the phase object is uniform the image obtained from defocusing microscopy is the image of curvature (Laplacian of the local thickness) of the phase object, while standard phase-contrast microscopy gives information about the thickness of the object. We made artificial phase objects and measured image contrasts with defocusing microscopy. Measured contrasts are in excellent agreement with our theoretical model. We use defocusing microscopy to study curvature fluctuations (ruffles) on the surface of macrophages (cell of the innate immune system), and try to correlate mechanical properties of macrophage surface and phagocytosis. We observe large coherent propagating structures: Their shape, speed, density are measured and curvature energy estimated. Inhomogeneities of cytoskeleton refractive index, curvature modulations due to thermal fluctuations and/or periodic changes in cytoskeleton-membrane interactions cause random fluctuations in image contrast. From the temporal and spatial contrast correlation functions, we obtain the decay time and correlation length of such fluctuations that are related to their size and the viscoelastic properties of the cytoskeleton. In order to associate the dynamics of cytoskeleton with the process of phagocytosis, we use an optical tweezers to grab a zymosan particle and put it into contact with the macrophage. We then measure the time for a single phagocytosis event. We add the drug cytochalasin *D* that depolymerizes the cytoskeleton F-actin network: It inhibits the large propagating coherent fluctuations on the cell surface, increases the relaxation time of cytoskeleton fluctuations, and increases the phagocytosis time. Our results suggest that the methods developed in this work can be of utility to assess the importance of cytoskeleton motility in the dynamics of cellular processes such as phagocytosis exhibited by macrophages.

DOI: 10.1103/PhysRevE.67.051904

PACS number(s): 87.64.Rr, 83.80.Lz, 05.40.-a

I. INTRODUCTION

A transparent object whose index of refraction is very close to the index of refraction of its embedding medium (a phase object) can become visible in an optical microscope by using the well-known Zernike's phase-contrast method. Changes in image intensity are proportional to the phase changes introduced by the phase object [1]. For a thin phase object with uniform index of refraction, phase-contrast microscopy then yields a measure of the phase object thickness $h(x,y)$. Another way of making phase objects visible in an optical microscope, but seldom used as an useful tool, is the defocusing method. The treatment of defocusing as a wave aberration has been considered by many authors [1–4]. Figure 1 shows how defocusing can make visible stains on a microscope glass slide (a) for positive defocusing, (b) in focus (object invisible), and (c) for negative defocusing. We revisited the theory of defocusing and apply it to our optical microscope with optics corrected at infinity. In our approximation, we obtain that the image contrast is proportional to the two-dimensional Laplacian of the phase difference introduced by the phase object and proportional to the amount of defocusing. For a phase object with uniform index of refraction, defocusing microscopy yields an image contrast propor-

tional to $\nabla^2 h(x,y)$, that is the curvature of the phase object if $|\nabla h(x,y)| \ll 1$. Under these conditions, the image obtained from defocusing microscopy is a portrait of the curvature of the phase object. Naturally, the same information can be obtained from the thickness $h(x,y)$ measured by phase-contrast microscopy. However, in the application that we will report here, we are interested in measuring the dynamics of cell surface fluctuations, where surface curvature is one of the main parameters. Therefore, with defocusing microscopy the images obtained are easier to analyze and are directly related to the parameter we want to measure.

The defocusing method using laser light was applied recently to study spatial and temporal fluctuations of optical microstructures of stratified seawater caused by grid turbulence [5]. Here, we apply defocusing microscopy to study



FIG. 1. Stains on a microscope coverglass: (a) for positive defocusing, (b) in focus (object invisible), and (c) for negative defocusing.

surface curvature fluctuations of macrophages, an important cell of the innate immune system. Engulfment of pathogens by professional phagocytic cells (macrophages) is one of the most primitive and important functions of the innate immune system. Phagocytosis is a very complex process where pathogens are recognized, internalized, and then digested by macrophages, through elaborate recognition and metabolic signaling paths [6–9]. A great deal of information about the biochemical aspects of this process is available in the literature. We are particularly interested how mechanical properties of cytoskeleton and cell surface fluctuations influence, and mediate the engulfment of particles and pathogens during phagocytosis.

We identify that the main surface fluctuations correspond to large coherent structures (kinklike structures) that propagate from the edge towards the nucleus of the cell. These large structures are probably responsible for the so-called centripetal motion observed in macrophages and in other cells [10]. We measure their shapes, amplitudes, velocity, and density in control macrophages and in macrophages treated with cytochalasin *D* (CyD), a drug that depolymerizes the *F*-actin network of the cytoskeleton. The amount and speed of these large structures decreases considerably with the addition of CyD. This characterization of surface fluctuations is important for any modeling of cell motility.

With an optical tweezers [11–13], we grab a zymosan particle, a model particle used in phagocytosis experiments, and put it into contact with a macrophage. We are then able to observe a single phagocytosis event. We videotape the process until the zymosan particle is completely engulfed and obtain the phagocytosis time. We observe a positive correlation between the amount of surface fluctuations of a single macrophage and phagocytosis time. Therefore, the method described here can be useful for an assessment of cytoskeleton cell activity that is important for phagocytosis.

This paper is organized as follows: in Sec. II, we present the theory of defocusing for our infinity corrected optical microscope; in Sec. III, we present experimental results of defocusing microscopy in constructed phase objects that confirms the theoretical analysis; in Sec. IV, we present the method of preparation of macrophages and discuss some other experimental aspects; in Sec. V, we present our results and discussions about the statistical characterization of surface fluctuations, viscoelastic properties of cytoskeleton and phagocytosis time; in Sec. VI, we present our conclusions; finally, in the Appendix, we show the mathematical derivations of the theory of defocusing microscopy presented in Sec. II.

II. THEORY OF DEFOCUSING

Our optical microscope is an inverted Nikon Eclipse TE300 with optics corrected at infinity. The objective conjugates the image of the object at infinity and a tube lens focuses the rays in the image plane to form the image. So, in our model of defocusing we are going to consider our microscope composed of two lenses: the infinity corrected objective with focal distance f_1 and a tube lens with focal distance f_2 separated by the distance d as shown in Fig. 2 [14]. We

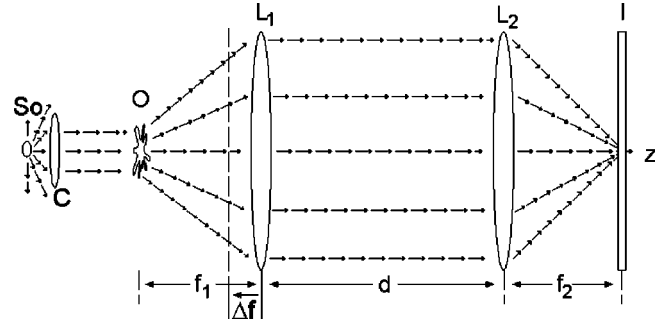


FIG. 2. Scheme of an infinity corrected microscope. S_o represents the light source, a tungsten lamp, C is the condenser that illuminates the object O , L_1 is the objective, L_2 is the tube lens, the image is conjugated in the image plane I , and we defocus the microscope by Δf .

defocus our microscope by moving the objective by a distance Δf in relation to the object: positive Δf means that the objective approaches the object, negative Δf otherwise. In our experiments, we use an oil immersion objective of 100X with numerical aperture $NA=1.4$ (CFI Plan Apochromat) and a bright field scheme with illumination provided by a tungsten lamp without frequency filters. Even though we use a broad-band light source, since the observed objects are very small (of the order of tens of microns) they are within a coherence area. This can be easily checked by using an object with a sharp edge; we clearly see the edge diffraction fringes as in coherent illumination. Therefore, one can use the mathematical techniques and procedures developed for coherent optics. Light from the object propagates through both lenses and form the image. In the Appendix, we describe the propagation of the light through our defocused microscope and the mathematical derivations that result in the following expression for the contrast of the defocused image:

$$C(\vec{\rho}) = \frac{I(\vec{\rho}) - I_0}{I_0} = \frac{\Delta f}{k} \nabla^2 \varphi(\vec{\rho}), \quad (1)$$

where $\varphi(\vec{\rho})$ is the phase difference introduced by the phase object and k is the light wave vector.

We notice that the image contrast can be positive or negative depending on the signs of Δf and $\nabla^2 \varphi(\vec{\rho})$. For a thin phase object

$$\varphi(\vec{\rho}) = k \Delta n h(\vec{\rho}), \quad (2)$$

where Δn is the difference between the refractive index of the phase object and its embedding medium, and $h(\vec{\rho})$ is the thickness of the phase object. The equation for the contrast can be rewritten as

$$C(\vec{\rho}) = \Delta f \nabla^2 [\Delta n h(\vec{\rho})]. \quad (3)$$

An interesting point in the above expression is that it does not depend explicitly on the wavelength of the incident light, what justifies the fact that we do not need frequency filtering in our illumination to use with this technique. The index of

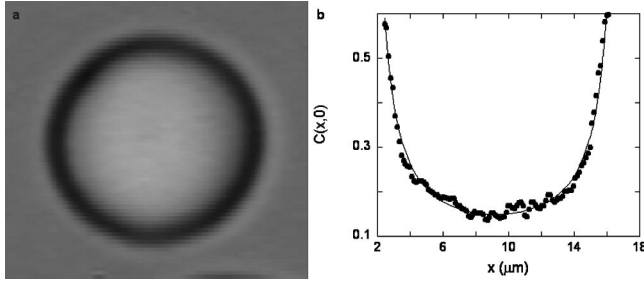


FIG. 3. (a) Image of a defocused spherical cap of polystyrene in water; (b) contrast fitted with Eq. (A17); from the fit $R=8.09 \pm 0.03 \mu\text{m}$.

refraction of the object is then the mean refractive index averaged over the incident wavelengths. Contrast can be obtained from $\nabla^2 h(\vec{\rho})$ and from $\nabla^2(\Delta n)$ in the case of phase objects with inhomogeneous index of refraction.

III. EXPERIMENTAL TEST OF THE DEFOCUSING MODEL

Since several approximations were made to have a simplified model of defocusing, an experimental test of the final expression for the contrast [Eq. (3)] is required. If we make thin phase objects with uniform refractive index (Δn constant), Eq. (3) can be written as

$$C(\vec{\rho}) = \Delta f \Delta n \nabla^2 h(\vec{\rho}). \quad (4)$$

Equation (4) has a simple physical interpretation. The contrast is the ratio between the amount of defocusing Δf and the local focal distance of the phase object that acts as a thin lens, since $\Delta n \nabla^2 h(\vec{\rho})$ is the lens-maker equation for the inverse focal distance. So, in this approximation the phase object behaves as a thin convergent or divergent lens. In order to make controlled phase objects, we use $1\text{-}\mu\text{m}$ -radius polystyrene beads as starting material from Polysciences Inc., with glass transition temperature of 100°C and refractive index of 1.600 for $\lambda = 589.3 \text{ nm}$ [15]. We put a drop of water solution of the beads on a glass slide (thickness $170 \mu\text{m}$) used in our microscope. After water evaporation the beads are stuck on the slide. There are aggregates of one to several beads. The slide is then put in an oven at 150°C for about 1 h. This temperature is enough to soften the beads and they take the shape of thin spherical caps, with different curvatures. After cooling the slide down it is used as the bottom of our Plexiglas sample cell. Therefore, we can make measurements on the polystyrene caps in air or in another medium. Figure 3(a) shows an image of the defocused spherical cap. For the spherical cap $h(x,y) = (R^2 - x^2 - y^2)^{1/2} - \text{const}$ and

$$\nabla^2 h(x,y) = - \left[\frac{2R^2 - x^2 - y^2}{(R^2 - x^2 - y^2)^{3/2}} \right]. \quad (5)$$

Taking the contrast along a diameter in Fig. 3(a) ($y=0$), the contrast can be written as

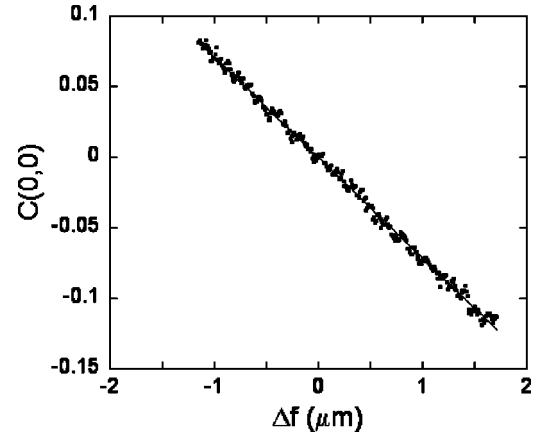


FIG. 4. Plot of $C(0,0)$ as a function of the defocusing for the cap of Fig. 3. The slope of the fit $S = \Delta n 2/R$ is $S = -0.0714 \pm 0.0002 \mu\text{m}^{-1}$.

$$C(x,0) = \Delta f \Delta n \left[\frac{2R^2 - x^2}{(R^2 - x^2)^{3/2}} \right]. \quad (6)$$

We use a positive sign in Eq. (6) because in our image analysis the gray levels are 255 for the darkest and zero for the whitest pixels. Figure 3(b) shows the measured contrast $C(x,0)$ (circles) and the fit using Eq. (6) (continuous line). From the fit one obtains the radius of curvature of the cap R and the coefficient $\Delta f \Delta n$. In addition, we can obtain the contrast

$$C(0,0) = \Delta f \Delta n \frac{2}{R}. \quad (7)$$

For each cap the defocusing Δf is varied and Fig. 4 shows a plot of $C(0,0)$ as a function of Δf . Beyond the limits shown in the plot, $C(0,0)$ is no longer a linear function of Δf . From each plot is extracted the slope S of this straight line that, from our model, is equal to $S = \Delta n 2/R$. Finally, Fig. 5 shows the plot of S as a function of $2/R$. If our model is quantita-

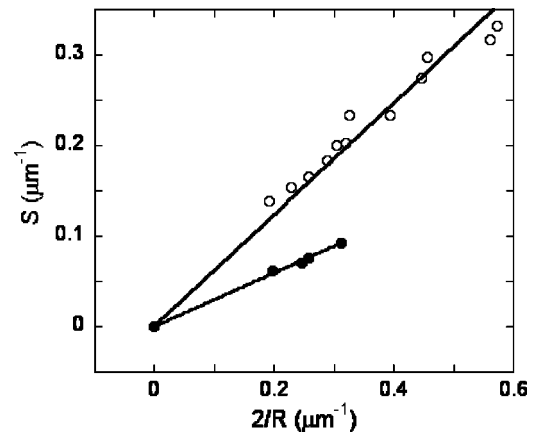


FIG. 5. Plot of $S = \Delta n 2/R$ as a function of the curvature $2/R$. The slope of this fit is the difference of refractive index between the polystyrene and the medium, for air (\circ) $\Delta n_a = 0.61 \pm 0.01$ and for water (\bullet) $\Delta n_w = 0.29 \pm 0.01$.

tively correct, the slope of this straight line should be in (○), the difference in index of refraction of the polystyrene and air ($\Delta n_a = 1.60 - 1 = 0.60$), and in (●) the difference in index of refraction of the polystyrene and water ($\Delta n_w = 1.60 - 1.33 = 0.27$). From the fits, we obtain $\Delta n_a = 0.61 \pm 0.01$ and $\Delta n_w = 0.29 \pm 0.01$ in good agreement with the predictions of our defocusing model.

IV. MATERIALS AND METHODS

A. Animals

Mice five to six weeks old (C57BL/6) were obtained from the animal house of Fundação Oswaldo Cruz (Rio de Janeiro, Brazil) and maintained under standard conditions in the animal house of the Centro de Pesquisas René Rachou da Fundação Oswaldo Cruz (Belo Horizonte, Brazil).

B. Macrophages preparation

Thioglycollate-elicited peritoneal macrophages were obtained from C57BL/6 by peritoneal washing [16]. Adherent macrophages were cultured at 37°C with 5% CO₂ in DMEM (Dulbeccos Modified Eagles Medium-Sigma) in a chamber made of a cylindrical Plexiglas glued on a microscope glass slide with torr seal (Varian Vacuum Products). The chamber can hold 1.5 ml of solution. After 20 h, the culture medium was replaced by the same medium with 10% of inactivated fetal bovin serum. Experiments were performed 2 h after the change of the medium. For the experiments with cytochalasin *D* (CyD sigma) cells were incubated with 100 nM of CyD 2 h or instantly before the experiments were performed.

C. Optical tweezers and videomicroscopy setup

We use a Nikon TE300 microscope with an oil immersion microscope objective with magnification of 100X and NA = 1.4. In all experiments, we use Köhler illumination for maximum uniformity of image intensity. To keep the temperature of the cell at 37°C, the objective is heated. Visualization is made with the same objective and recorded with a digital camera (DAGE MTI) and a videocassette recorder (EVO 9650-SONY). The optical tweezers consists of a collimated beam of infrared laser (SDL 5280) that goes through the objective. Details of our experimental setup can be obtained from Viana *et al.* [13].

D. Zymosan preparation and measurement of phagocytosis time

Zymosan A (sigma) was washed two times with phosphate buffered saline (PBS) and incubated with fetal bovine serum not inactivated for at least 2 h before the experiment. Using the optical tweezers a zymosan particle is then put into contact with a macrophage near its edge. The time of phagocytosis is defined as the time that the cytoskeleton takes to surround the particle [24].

E. Image analysis

Recorded images were digitized as movies with eight-bits graylevels, using a data-translation frame grabber and stored in a PC microcomputer. The movies of the macrophages were analyzed with the program NIH-IMAGEJ. Correlation

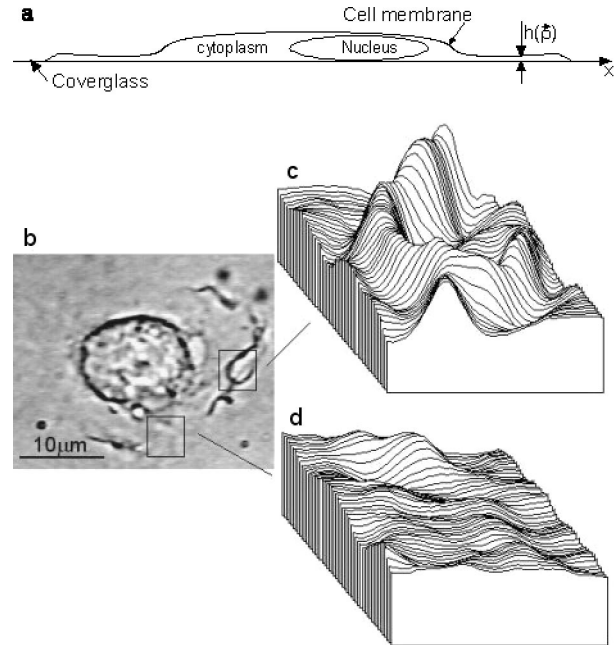


FIG. 6. (a) Sketch of a macrophage adhered on glass. (b) Image of a macrophage obtained with microscope defocusing of $\Delta f = 1 \mu\text{m}$ [25]. (c) Contrast profile [proportional to $\nabla^2 h(x,y)$] of kinklike structure propagating from the edge toward the nucleus of the cell. (d) Contrast profile of small random fluctuations.

functions and PDFs (probability distribution functions) data were obtained with java applets that we have made for the IMAGEJ program.

V. RESULTS AND DISCUSSION

Plasma membrane separates the cell constituents from the external environment. Plasma membrane is a continuous elastic medium, therefore elastic energy is spent to drive fluctuations on the surface of the cell. Cells have membrane reservoirs to face the enormous morphological changes required for their functioning [17]. Because of that, cell surface tension is small and membrane curvature is likely to be the most important contribution to the elastic energy of cell surface [18]. Therefore, it is reasonable to think that we can have an assessment of cytoskeleton macrophage activity by measuring curvature fluctuations (ruffles). Hence, defocusing microscopy discussed before is a good technique to study cell surface fluctuations because the images obtained are related to surface curvature, resulting in simpler images as compared to phase-contrast microscopy, facilitating the image analysis. Single macrophages using defocusing microscopy are filmed for at least 2 h, such that enough information is obtained to perform the statistical analysis that will be described below. We observe two main types of contrast fluctuations: small random fluctuations that permeate the whole cell and large coherent structures that propagate from the edge towards the nucleus of the cell. Figure 6(a) presents a sketch of a macrophage adhered on a glass substrate and Fig. 6(b) an image of a macrophage obtained using defocus-

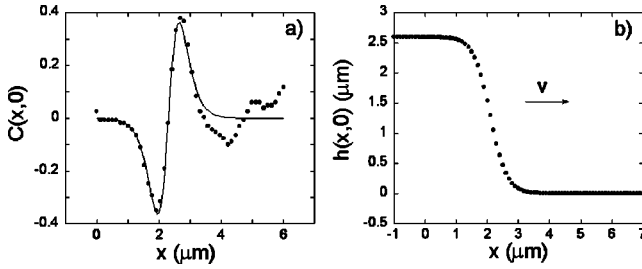


FIG. 7. (a) One-dimensional contrast profile of a propagating structure along the direction of propagation. This profile is well fit by Eq. (9) with $\Delta f = 1 \mu\text{m}$, $\Delta n = 0.1$ with the kink form of Eq. (8) resulting in $h_0 = 2.6 \mu\text{m}$ and $w = 0.53 \mu\text{m}$. (b) Example of the kink calculated using Eq. (8) with the parameters found in the fit.

ing microscopy with $\Delta f = 1 \mu\text{m}$. Surface contrast plots are also shown for regions with large and small fluctuations.

A. Large coherent structures

We observe mainly two types of large coherent structures: kinklike and Gaussian-like structures. In Fig. 7(a), we show the contrast as a function of the distance along the direction of propagation of a large structure, let us say x direction. If we assume a kinklike form [showed in Fig. 7(b)] for this propagating structure such that

$$h(x,y) = \frac{h_0}{2} \left[1 - \tanh\left(\frac{x-Vt}{w}\right) \right], \quad (8)$$

where h_0 is its amplitude, w width, V speed, and considering that the index of refraction of the cytoskeleton is on average uniform, an expression for the kink contrast can be obtained using Eq. (4),

$$C(x,y) = \frac{h_0}{w^2} \Delta f \Delta n \left[\tanh\left(\frac{x-Vt}{w}\right) - \tanh^3\left(\frac{x-Vt}{w}\right) \right]. \quad (9)$$

In Fig. 7(a) the dots are the experimental points and the continuous line is the fit using Eq. (9) for a particular time t . From this fit and using $\Delta f = 1 \mu\text{m}$ and $\Delta n = 0.1$ [19], we obtain $h_0 = 2.6 \mu\text{m}$ and $w = 0.53 \mu\text{m}$. Curvature energy of the kink can be calculated using the expression given below [18,20],

$$U_c = \frac{k_c}{2} \int dy \int dx \frac{\left(\frac{d^2h}{dx^2}\right)^2}{\left(1 + \left|\frac{dh}{dx}\right|^2\right)^3}, \quad (10)$$

where k_c is the bending stiffness and we have used the exact expression for curvature. The membrane-cytoskeleton adhesion will have a pronounced influence on the bending stiffness, however, we can have a lower bound estimate for the curvature energy using the bending stiffness of simple membranes, typically around 10^{-12} erg [21]. In this case, the curvature energy of the kink from Eq. (8), with parameters $h_0 = 2.6 \mu\text{m}$, $w = 0.53 \mu\text{m}$, and size along the y direction

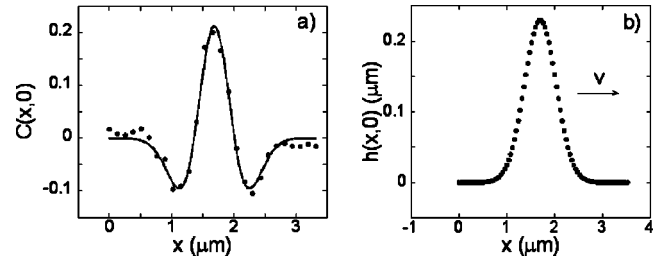


FIG. 8. (a) One-dimensional contrast profile of propagating structure along the direction of propagation. This profile is well fit by the Laplacian of the Gaussian form of Eq. (11) resulting in $h_0 = 0.23 \mu\text{m}$ and $w = 0.33 \mu\text{m}$. (b) Example of Gaussian profile calculated using Eq. (11) with the parameters found in the fit.

equal to $5 \mu\text{m}$ gives $U_c \approx 3.8 \times 10^{-12}$ erg, which is around 100 times the thermal energy. Hence, to make such large structures, the cell spends a considerable amount of energy. Similar calculations can be done for a Gaussian-like structure where we assume the profile below,

$$h(x,y) = h_0 e^{-(x-Vt)^2/2w^2}, \quad (11)$$

shown in Fig. 8(b). In Fig. 8(a) the dots are the experimental points and the continuous line is the fit for the contrast using the 2D Laplacian of the Gaussian profile above. The results are $h_0 = 0.23 \mu\text{m}$, $w = 0.33 \mu\text{m}$, and size along the y direction equal to $5 \mu\text{m}$ gives $U_c \approx 4.3 \times 10^{-12}$ erg, which is around 100 times the thermal energy. The average speed for the large structures is $\langle V \rangle = 3.5 \pm 0.7 \mu\text{m}/\text{min}$. By measuring the average amount of such large structures, we can infer how much curvature energy is involved in the process. Then the amount and speed of such structures can be a measure by macrophage cytoskeleton activity. From now on, we will refer to these large coherent structures as kinklike structures.

B. Random fluctuations

To characterize the random contrast fluctuations that permeate the whole cell, we calculate contrast temporal and spatial correlation functions from the digitized images of a macrophage. Time autocorrelation function $\langle C(0)C(t) \rangle$ is obtained from the contrast of every pixel (pixel length = $0.13 \mu\text{m}$) in different times, averaged over several pixels of a chosen region. The spatial correlation function $\langle C(0)C(r) \rangle$ is obtained from the simultaneous value of the contrast in different pixels and the average is done over many video frames. In Fig. 9(a) is shown a time autocorrelation function fitted to a single exponential, with a relaxation time of $\tau = 4.5$ s. A surprising result is the reproducibility of the relaxation time given that this is a biological system: for 30 different macrophages and for various different positions in each macrophage the relaxation time was $\tau = 5 \pm 1$ s. In Fig. 9(b) is shown a spatial correlation function that was fit to a single exponential with a correlation length of $\xi = 0.26 \mu\text{m}$, and averaging over many measurements $\xi = 0.25 \pm 0.02 \mu\text{m}$. This value is just the resolution limit of our objective of 100X and $\text{NA} = 1.4$. Therefore, whatever is causing these small random fluctuations its typical size is smaller than $0.25 \mu\text{m}$. These fluctuation can be caused by

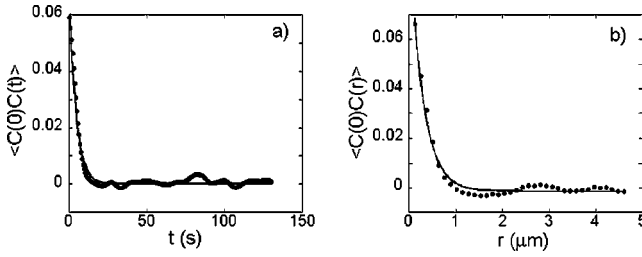


FIG. 9. (a) Temporal contrast autocorrelation function of random fluctuations with relaxation time $t = 4.5$ s. (b) Spatial contrast correlation function of random fluctuations with correlation length $\xi = 0.26 \mu\text{m}$ that corresponds to the optical resolution of our microscope.

small surface curvature fluctuations or by inhomogeneities of the index of refraction inside the cell via the term $\nabla^2(\Delta n)$ in the contrast. Bausch *et al.* [22] measured the viscoelastic properties of the cytoskeleton of macrophages with a microrheometer and provided evidence that the whole cytoskeleton is composed of clusters of densely packed and/or strong crosslinked filaments (smaller than $0.25 \mu\text{m}$) separated by very soft or sol-like regions. Since there are thermal fluctuations on all length scales [20], at the present stage, we cannot separate the contributions caused by inhomogeneities in the refractive index, curvature modulations from thermal fluctuations and/or periodic changes in cytoskeleton-membrane interactions.

C. Probability distribution function

An additional statistical characterization can be done by constructing the probability distribution function (PDF) of contrast fluctuations. To do that, we construct a function of the number of times $N(C)$ that a particular contrast C occurred as a function of C . In Fig. 10(a), we show a plot of $N(C)$ as a function of C normalized by the standard deviation ($\sqrt{\langle \Delta C^2 \rangle}$), for a macrophage. We are able to fit this curve by a sum of a Gaussian plus and an exponential function: the Gaussian part is related to the small random fluctuations and the long exponential tails related to the large coherent fluctuations

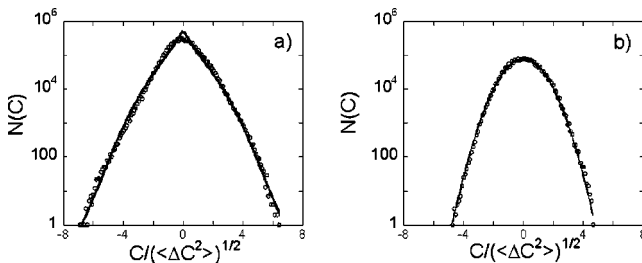


FIG. 10. Probability distribution functions (PDFs) of contrast fluctuations. (a) Before the addition of the cytoskeletal drug *CyD*, where the PDF clearly shows long exponential tails and (b) 40 min after the addition of 100 nM of *CyD*, where the PDF becomes more Gaussian indicating the decrease of the relative kink density as described in the text.

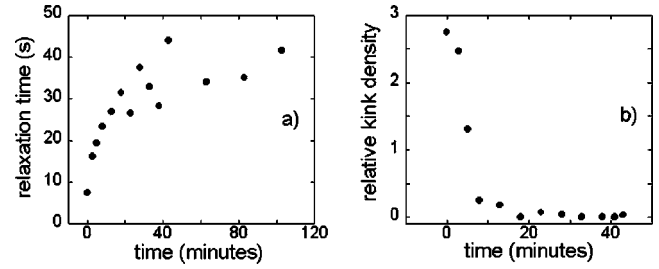


FIG. 11. (a) Plot of the relaxation time of random fluctuations as a function of time after the addition of 100 nM of *CyD*. (b) Plot of the relative density of kinks as a function of time after the addition of 100 nM of *CyD*.

$$N(C) = N_0 \left[\frac{\exp\left(\frac{-C^2}{2\sigma^2}\right)}{\sqrt{2\pi\sigma^2}} + f_K \frac{\exp\left(\frac{-|C|}{\alpha}\right)}{2\alpha} \right], \quad (12)$$

where N_0 , σ , and α are constants and f_K is the fraction of large fluctuations as compared to the small fluctuations. We then name f_K as the relative kink density. In Fig. 10(a), the squares are the experimental points and the continuous line is the fit using Eq. (12) and from the fit $f_K = 2.8$. A theoretical derivation for the kind of PDFs we have observed is by itself an interesting task, since this is a nonlinear and far from equilibrium dynamical system. Hence, an assessment of the macrophage cytoskeleton activity can be obtained from the comparison between the kink densities of a control macrophage and a macrophage under study. Also we can study the time evolution of activity after the administration of some drug to the macrophage. That is what we are going to do in the following section by adding the cytoskeleton drug cytochalasin *D*.

D. Macrophage with cytochalasin *D*

Cytochalasin is a drug that depolymerizes the cytoskeleton *F*-actin network changing its viscoelastic properties. Möller *et al.* [23] showed that the main effect of *CyD* is to increase the cytoskeleton viscosity, while changing little the cytoskeletal stiffness. After the addition of 100 nM of *CyD*, we measure the relaxation time of random fluctuations, the average speed of the kinklike structures, and the relative kink density. In Fig. 10(b), we show the PDF data 40 min after the addition of *CyD*. The PDF became more Gaussian and from the fit we obtain $f_K = 0.03$. It indicates that the amount of kinks has decreased considerably. The average speed of kinks has also decreased to the value $\langle V \rangle = 0.5 \pm 0.2 \mu\text{m}/\text{min}$. In Fig. 11(a) is shown the relaxation time of random fluctuations as a function of time after the addition of *CyD*. A considerable increase in relaxation time is observed probably due to the increase in viscosity of the cytoskeleton. In Fig. 11(b) is shown the density of kinks as a function of the time after the addition of *CyD*. *CyD* inhibits the production of the large kinklike fluctuations.

E. Phagocytosis time of zymosan

With an optical tweezers mounted in our microscope we grab a zymosan particle ($\sim 4 \mu\text{m}$) and feed a macrophage,

TABLE I. Numbers in parentheses are the number of samples used in the averages [24].

CyD (nM)	Kink speed ($\mu\text{m}/\text{min}$)	Kink density	Relaxation time (s)	Phagocytosis time (min)
0.0	$3.5 \pm 0.7(7)$	$2.5 \pm 1.5(5)$	$5 \pm 1(30)$	$3 \pm 2(26)$
100	$0.5 \pm 0.2(7)$	$0.02 \pm 0.02(9)$	$40 \pm 10(9)$	$> 120(2)$

and videotape the process of phagocytosis. We then measure the time for complete engulfment of zymosan by the macrophage (phagocytosis time). From the images, as a local effect, we observe a slight increase in the kink activity around the zymosan particle during phagocytosis. Phagocytosis time increases considerably from 3 min to more than 2 h due to CyD. Results are displayed in Table I. Since phagocytosis time increased more than linearly with the relaxation time, which is an indication of how much the overall cytoskeleton motion has slowed down, the kink density seems to represent the more dramatic change of cytoskeleton activity that is related to phagocytosis.

VI. CONCLUSIONS

We revisited the theory of defocusing and showed that for our infinity corrected microscope and for the paraxial approximation, the contrast of a phase object observed with defocusing microscopy is proportional to the amount of defocusing and to the 2D Laplacian of the phase difference introduced by the phase object. Therefore, defocusing microscopy is a convenient technique for measuring curvature of phase objects. We constructed artificial phase objects to test quantitatively our expression for the contrast. Experiment and theory agree quite well. We then use defocusing microscopy to study surface fluctuations of macrophages. We observe mainly two types of macrophage fluctuations: large surface propagating coherent structures and small random fluctuations. We measure shape, speed, and relative density of these large propagating structures and make an estimate of their curvature energy. We measure relaxation time and correlation length associated to these random fluctuations, that may be caused by inhomogeneities in the refractive index, curvature modulations from thermal fluctuations and/or periodic changes in cytoskeleton-membrane interactions. At the present stage, we cannot single out each one of these contributions. With an optical tweezers we grab a single zymosan particle and put it into contact with a macrophage. We then measure the phagocytosis time for each single event. All measurements were repeated after the addition of the cytoskeleton drug cytochalasin *D*. Relaxation time of random fluctuations increases indicating that the internal motion of the cytoskeleton has slowed down; speed and density of the large propagating structures decreases considerably indicating much less surface activity; phagocytosis time increases considerably. These results suggest that from the properties and density of the large kinklike structures, we have an assessment of surface cytoskeleton activity that is correlated with phagocytosis. Additional experiments are required to decide if these nonlocal large structures participate directly

to facilitate the phagocytosis process or if they just reflect the overall activity of macrophage cytoskeleton.

ACKNOWLEDGMENTS

We acknowledge helpful suggestions from F. Plentz for the preparation of the artificial phase objects. This work was supported by the Brazilian Agencies Fundação de Amparo à Pesquisa do Estado de Minas Gerais (FAPEMIG), Conselho Nacional de Desenvolvimento Científico e Tecnológico (CNPq), FINEP-PRONEX, and Instituto do Milênio de Nanociência-MCT.

APPENDIX

We will use the formalism of the angular spectrum to describe the propagation of the light through our microscope [2]. In this formalism, the electric field of a linear polarized light propagating along the z direction with angular components in the xy plane can be represented by its Fourier transform in the xy plane as

$$E(\vec{\rho}, z) = \frac{1}{(2\pi)^2} \int A(\vec{q}, z) e^{i\vec{q} \cdot \vec{\rho}} d\vec{q}, \quad (\text{A1})$$

where $\vec{\rho} = x\hat{i} + y\hat{j}$ and $\vec{q} = k_x\hat{i} + k_y\hat{j}$. The inverse Fourier transform gives

$$A(\vec{q}, z) = \int E(\vec{\rho}, z) e^{-i\vec{q} \cdot \vec{\rho}} d\vec{\rho}, \quad (\text{A2})$$

where $A(\vec{q}, z)$ is the angular spectrum. The free space propagation of the angular spectrum from position $z=0$ up to a position z , in the paraxial approximation where $|\vec{q}| \ll |\vec{k}|$, is given by [2]

$$A(\vec{q}, z) = A(\vec{q}, 0) e^{ikz} e^{-i(q^2/2k)z}, \quad (\text{A3})$$

where k is the magnitude of the wave vector of the light. The propagation of the angular spectrum across one lens is given by

$$A_1(\vec{q}) = \frac{f}{2\pi ik} \int A_0(\vec{\xi}) e^{i(f/2k)(\vec{q}-\vec{\xi})^2} d\vec{\xi}, \quad (\text{A4})$$

where f is the focal distance of the lens. To compute the final angular spectrum and, consequently, the electric field of the light through our defocused microscope, we have to use Eqs. (A3) and (A4) in five steps to propagate the angular spectrum: (1) from the position of the object ($z=0$) through a distance $f_1 - \Delta f$ up to the objective; (2) across the objective of the focal distance f_1 ; (3) from the objective through a distance $d + \Delta f$ up to the tube lens; (4) across the tube lens of the focal distance f_2 ; (5) from the tube lens through a distance f_2 up to the focal plane. The resulting angular spectrum after each step is given below. After step (1),

$$A_1 = A_0(\vec{q}) e^{ik(f_1 - \Delta f)} e^{-i(f_1/2k)q^2} e^{i(\Delta f/2k)q^2}. \quad (\text{A5})$$

After step (2),

$$A_2 = \frac{f_1}{2\pi ik} e^{ik(f_1 - \Delta f)} e^{i(f_1/2k)q^2} \times \int A_0(\vec{\xi}) e^{i(\Delta f/2k)\xi^2} e^{-i(f_1/k)\vec{q} \cdot \vec{\xi}} d\vec{\xi}. \quad (\text{A6})$$

Calling $B_0(\vec{q}) = A_0(\vec{\xi}) e^{i(\Delta f/2k)q^2}$ and its inverse transform as $b_0(\vec{\rho}) = F^{-1}\{B_0(\vec{q})\}$, we have

$$A_2 = \frac{2\pi f_1}{ik} e^{ik(f_1 - \Delta f)} e^{i(f_1/2k)q^2} b_0\left(-\frac{f_1}{k}\vec{q}\right). \quad (\text{A7})$$

After step (3),

$$A_3 = \frac{2\pi f_1}{ik} e^{ik(f_1 + d)} e^{-i(f_2/2k)q^2} b_0\left(-\frac{f_1}{k}\vec{q}\right). \quad (\text{A8})$$

After step (4),

$$A_4 = -\frac{f_1 f_2}{k^2} e^{ik(f_1 + d)} e^{i(f_2/2k)q^2} \int b_0\left(-\frac{f_1}{k}\vec{\xi}\right) \times e^{i[(f_1 + f_2 - d - \Delta f)/2k]\xi^2} e^{-i(f_2/k)\vec{q} \cdot \vec{\xi}} d\vec{\xi}. \quad (\text{A9})$$

After step (5),

$$A_5 = -\frac{f_1 f_2}{k^2} e^{ik(f_1 + f_2 + d)} \int b_0\left(-\frac{f_1}{k}\vec{\xi}\right) \times e^{i[(f_1 + f_2 - d - \Delta f)/2k]\xi^2} e^{-i(f_2/k)\vec{q} \cdot \vec{\xi}} d\vec{\xi}. \quad (\text{A10})$$

To simplify this expression, we made the following variable change, $\vec{\xi}' = -(f_1/k)\vec{\xi}$, to obtain

$$A_5 = -\frac{f_2}{f_1} e^{ik(f_1 + f_2 + d)} \times \int b_0(\vec{\xi}') e^{i[(f_1 + f_2 - d - \Delta f)k/2f_1^2]\xi'^2} e^{i(f_2/f_1)\vec{q} \cdot \vec{\xi}'} d\vec{\xi}'. \quad (\text{A11})$$

To obtain the electric field, we perform the inverse Fourier transform of Eq. (A11),

$$E(\vec{\rho}) = -\frac{f_2}{(2\pi)^2 f_1} e^{ik(f_1 + f_2 + d)} \times \int \int e^{i[(f_2/f_1)\vec{\xi}' + \vec{\rho}] \cdot \vec{q}} d\vec{q} b_0(\vec{\xi}') \times e^{i[(f_1 + f_2 - d - \Delta f)k/2f_1^2]\xi'^2} d\vec{\xi}'. \quad (\text{A12})$$

Using the definition of the Dirac- δ function, $\delta(\vec{\rho}) = [1/(2\pi)^2] \int e^{-i\vec{\rho} \cdot \vec{q}} d\vec{q}$, Eq. (A12) can be simplified:

$$E(\vec{\rho}) = -\frac{f_1}{f_2} e^{ik(f_1 + f_2 + d)} b_0\left(-\frac{f_1}{f_2}\vec{\rho}\right) e^{i[(f_1 + f_2 - d - \Delta f)k/2f_2^2]\rho^2}. \quad (\text{A13})$$

By substituting $b_0[-(f_1/f_2)\vec{\rho}]$ in Eq. (A13) one obtains

$$E(\vec{\rho}) = -\frac{f_1}{(2\pi)^2 f_2} e^{ik(f_1 + f_2 + d)} e^{i[(f_1 + f_2 - d - \Delta f)k/2f_2^2]\rho^2} \times \int A_0(\vec{q}) e^{i(\Delta f/2k)q^2} e^{i[-(f_1/f_2)\vec{\rho}] \cdot \vec{q}} d\vec{q}. \quad (\text{A14})$$

The negative sign of the term $-(f_1/f_2)\vec{\rho}$ in the phase factor inside the integral means that the image is inverted and the ratio between the focal distances gives the magnification. Once the scale of the microscope is calibrated one can rewrite the expression above in terms of the spatial coordinates of the object, replacing $-(f_1/f_2)\vec{\rho}$ by $\vec{\rho}$. Then,

$$E(\vec{\rho}) = e^{i\alpha} \frac{1}{(2\pi)^2} \int A_0(\vec{q}) e^{i(\Delta f/2k)q^2} e^{i\vec{\rho} \cdot \vec{q}} d\vec{q}, \quad (\text{A15})$$

where

$$e^{i\alpha} = e^{ik(f_1 + f_2 + d)} e^{i[(f_1 + f_2 - d - \Delta f)k/2f_2^2]\rho^2}. \quad (\text{A16})$$

Unless a phase factor (A15) is the same one reported by Soroko for a confocal laser system [4]. In the derivation of Eq. (A15), we did not consider the finite size of the objective entrance pupil. Therefore, this expression is valid for angular wave vectors $q < q_M$ where $q_M = kNA/n$ with $n = 1.48$ for the refractive index of the immersion oil used and $NA = 1.4$, such that $q_M = 0.95k$. It means that if the paraxial condition is satisfied, the approximation of infinite entrance pupil is automatically satisfied in our objective. Following the procedure described by Soroko [4] and for small defocusing, such that $(\Delta f/2k)q_0^2 \ll 1$ where q_0 is the largest spatial wave vector of the object, we can expand the quadratic phase term inside the integral of Eq. (A15) as

$$e^{i(\Delta f/2k)q^2} = 1 + i \frac{\Delta f}{2k} q^2, \quad (\text{A17})$$

and obtain

$$E(\vec{\rho}) = e^{i\alpha} \frac{1}{(2\pi)^2} \left[\int A_0(\vec{q}) e^{i\vec{q} \cdot \vec{\rho}} d\vec{q} + i \frac{\Delta f}{2k} \int A_0(\vec{q}) q^2 e^{i\vec{q} \cdot \vec{\rho}} d\vec{q} \right]. \quad (\text{A18})$$

Utilizing the expansion for the electric field given by Eq. (A1), we obtain that

$$\nabla^2 E_0(\vec{\rho}) = \frac{-1}{(2\pi)^2} \int A_0(\vec{q}) q^2 e^{i\vec{q} \cdot \vec{\rho}} d\vec{q}. \quad (\text{A19})$$

Substituting Eqs. (A19) and (A1) into Eq. (A18), we obtain the expression for the electric field for the defocused image as

$$E(\vec{\rho}) = e^{i\alpha} \left[E_0(\vec{\rho}) - i \frac{\Delta f}{2k} \nabla^2 E_0(\vec{\rho}) \right]. \quad (\text{A20})$$

By assuming that the object is illuminated by a plane wave light propagating along the direction z with amplitude E_0 , the electric field of this light after passing the phase object can be written as

$$E_0(\vec{\rho}) = E_0 e^{i\varphi(\vec{\rho})}, \quad (\text{A21})$$

where $\varphi(\vec{\rho})$ is the phase difference introduced by the phase object.

Substituting Eq. (A21) into Eq. (A20) we obtain

$$E(\vec{\rho}) = e^{i\alpha} E_0 e^{i\varphi(\vec{\rho})} \left[1 + i \frac{\Delta f}{2k} [\nabla \varphi(\vec{\rho})]^2 + \frac{\Delta f}{2k} \nabla^2 \varphi(\vec{\rho}) \right]. \quad (\text{A22})$$

The image intensity is $I(\vec{\rho}) \propto |E(\vec{\rho})|^2$. If we only keep terms up to the first order in Δf , we obtain

$$I(\vec{\rho}) = I_0 + I_0 \frac{\Delta f}{k} \nabla^2 \varphi(\vec{\rho}), \quad (\text{A23})$$

where $I_0 \propto |E_0|^2$.

Due to a mistake in his expansion, the result of Soroko [4] for Eq. (A23) is different than ours. Finally, we can obtain an expression for the contrast of the defocused image as

$$C(\vec{\rho}) = \frac{I(\vec{\rho}) - I_0}{I_0} = \frac{\Delta f}{k} \nabla^2 \varphi(\vec{\rho}). \quad (\text{A24})$$

-
- [1] M. Born and E. Wolf, *Principles of Optics*, 7th ed. (Cambridge University Press, New York, 1999).
- [2] J.W. Goodman, *Introduction to Fourier Optics*, 2nd ed. (McGraw-Hill, Singapore, 1996).
- [3] P.A. Stokseth, *J. Opt. Soc. Am.* **59**, 1314 (1969).
- [4] L.M. Soroko, *Holography and Coherent Optics* (Plenum Press, New York, 1980).
- [5] B.N. Grudin, E.L. Kuleshov, V.S. Plotnikon, and V.K. Fishchenko, *Izv., Acad. Sci., USSR, Atmos. Oceanic Phys.* **37**, 247 (2001).
- [6] D.M. Underhill and A. Ozinsky, *Annu. Rev. Immunol.* **20**, 825 (2002).
- [7] F. Castelano, P. Chavrier, and E. Caron, *Semin. Immunol.* **13**, 347 (2001).
- [8] A. Aderem and D.M. Underhill, *Annu. Rev. Immunol.* **17**, 593 (1999).
- [9] R.C. May and L.M. Machesky, *J. Cell. Sci.* **114**, 1061 (1999).
- [10] A. Caspi, O. Yeager, I. Grosheva, A.D. Bershadsky, and M. Elbaum, *Biophys. J.* **81**, 1990 (2001).
- [11] A. Ashkin and J.M. Dziedzic, *Science* **235**, 1517 (1987).
- [12] K. Svoboda and S.M. Block, *Annu. Rev. Biophys. Biomol. Struct.* **23**, 247 (1994).
- [13] N.B. Viana, R.T.S. Freire, and O.N. Mesquita, *Phys. Rev. E* **65**, 041921 (2002).
- [14] M. Pluta, *Advanced Light Microscopy* (Elsevier Science, New York, 1988), Vol. 1.
- [15] Polysciences, Inc., Technical Data Sheet 238, site <http://www.polysciences.com/shop/assets/datasheets/238.pdf>
- [16] M.M. Camargo, I.C. Almeida, M.E.S. Pereira, M.A.J. Ferguson, R.L. Travassos, and R.T. Gazzinelli, *J. Immunol.* **158**, 5890 (1987).
- [17] Drazen Raucher and Michael P. Sheetz, *Biophys. J.* **77**, 1992 (1999).
- [18] W. Helfrich, *Z. Naturforsch. C* **28C**, 693 (1973).
- [19] J. Bereiter-Hahn, C.H. Fox, and B. Thorell, *J. Cell Biol.* **82**, 767 (1979) measured by reflection microscopy the value $\Delta n \approx 0.05$. In the ruffles, the index of refraction may be larger because of the increase of F -actin density. We estimate its value with defocusing microscopy by adding to the macrophage medium glycerine in different amounts. We measure the index of refraction of the medium with different amounts of glycerine with a refractometer. Around the concentration where the contrast changes from positive to negative, we estimate the index of refraction of the ruffles cytoskeleton and obtain $\Delta n \sim 0.1$.
- [20] S. Leibler, in *Proceedings of the Fifth Jerusalem Winter School, 1987/1988*, edited by D.R. Nelson, T. Pirani, and S. Weinberg (Springer, Berlin, 1989).
- [21] M. Bloom, E. Evans, and O.G. Mouritsen, *Q. Rev. Biophys.* **24**, 293 (1991).
- [22] A.R. Bausch, W. Möller, and E. Sackmann, *Biophys. J.* **76**, 573 (1999).
- [23] W. Möller, I. Nemoto, T. Matsuzaki, T. Hofer, and J. Heyder, *Biophys. J.* **79**, 720 (2000).
- [24] A movie of a phagocytosis event 12.5 times faster can be seen at the site <http://www.fisica.ufmg.br/~estatexp/zymosan.mpg>
- [25] A movie of the macrophage 16.2 times faster can be seen at the site <http://www.fisica.ufmg.br/~estatexp/macrophage.mpg>